The Boundary Layer on an Axisymmetric Body With and Without Spin

Jerome T. Kegelman,* Robert C. Nelson,† and Thomas J. Mueller‡
University of Notre Dame, Notre Dame, Indiana

The results from an experimental study of the boundary layer surrounding an axisymmetric model consisting of a 3-caliber secant ogive nose, a 2-caliber cylindrical midsection, and a 1-caliber 7-deg conical boattail are presented. Low-speed flow visualization data at zero angle of attack are shown for Reynolds numbers between 315,000 and 1,030,000 (based upon total body length), and ratios of peripheral to freestream velocity between 0 and 1.67. The smoke-flow photographs display the various stages of transition of the boundary layer. In addition, pressure distribution data are included for the nonspinning case. The pressure data are used in conjunction with the photographic data to present a "physical" picture of the boundary-layer development on the model.

Nomenclature

C_p = pressure coefficient, $(P-P_\infty)/\frac{1}{2}\rho U_\infty^2$
D = diameter of cylindrical section and equal to 1 caliber
f = frequency
L = total length of the body
P = local static pressure
p = spin rate, rad/s
P_∞ = freestream static pressure
Re_L = Reynolds number based on model length, $= U_\infty L/\nu$
U_∞ = freestream velocity
V = surface velocity of midsection, $= pD/2$
V/U_∞ = ratio of peripheral to freestream velocity
Z = axial distance measured from nose of body
δ = boundary-layer thickness at $U = 0.99U_\infty$
θ = striation angle measured from smoke photograph from a horizontal plane through the model axis
λ_{TS} = wavelength of Tollmien-Schlichting waves
ρ = density
ν = kinematic viscosity

Introduction

THE flight dynamics of a spinning body of revolution can be influenced significantly by the Magnus forces and moments acting on the body. These forces and moments are major contributors to the inaccuracies and dispersion of spin-stabilized projectiles as well as the dominant mechanisms for producing flight instabilities. As a result, a great deal of research has been conducted to determine the parameters affecting the Magnus forces. Experimental investigations have shown the Magnus force to be a function of Reynolds number, Mach number, ratio of peripheral to freestream velocity, angle of attack, and body geometry. Although progress has been made in both the theoretical and experimental aspects of this problem,[1-9] there appears to be a need to improve our physical understanding of the basic flow components.

The Magnus force originates in the boundary layer and, therefore, is directly related to the boundary-layer characteristics. That is, the magnitude of the Magnus force depends upon whether the boundary layer is predominantly laminar or turbulent.[8] When the flow is laminar, reasonably accurate numerical calculations can be obtained for almost any situation; i.e., compressible, incompressible, two-dimensional, three-dimensional, steady, or unsteady. The only practical limitations are the size and speed of the digital computer or the funds available to obtain a result with the desired accuracy. Using semiempirical methods, fully turbulent flows may also be calculated in many cases within the accuracy necessary for engineering purposes. The physical events which the fluid encounters in changing from a laminar to a fully turbulent flow—the transition process—presently cannot be determined by theoretical or numerical methods. The principal reason for this deficiency is that our understanding of this complex phenomenon is not complete enough to form a detailed theoretical model. Although there are significant differences between compressible and incompressible boundary-layer flows with regard to growth, separation, and the stability of laminar layers, useful ideas of fundamental importance may be obtained by studying incompressible flows. The detailed results and subsequent understanding obtained at low speeds will be useful in interpreting results in high-speed flows.[10-13]

The study presently being conducted at the University of Notre Dame is an extension of the work of Refs. 1 and 14-17. The experimental investigation is being directed toward obtaining an understanding of the effects of spin on the boundary-layer characteristics of secant ogive nose axisymmetric bodies. To accomplish this task, a combined visual and pressure measurement study was initiated. The ultimate objective of this investigation is to present a

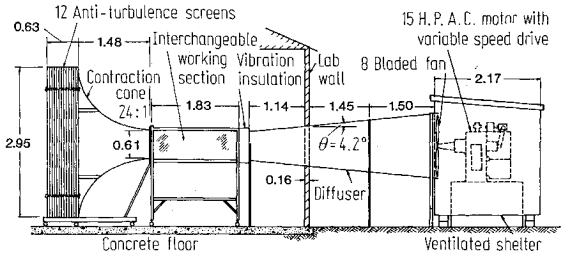

Fig. 1 Low-turbulence subsonic smoke tunnel with axisymmetric body. (All dimensions in meters.)

Presented as Paper 80-1584 at the AIAA Atmospheric Flight Mechanics Conference, Danvers, Mass., Aug. 11-13, 1980; submitted Sept. 24, 1980; revision received Feb. 15, 1983.

*Graduate Assistant, Dept. of Aerospace and Mechanical Engineering; presently, Research Scientist, McDonnell Douglas Corp., St. Louis, Mo. Member AIAA.

†Associate Professor, Dept. of Aerospace and Mechanical Engineering. Associate Fellow AIAA.

‡Professor, Dept. of Aerospace and Mechanical Engineering. Associate Fellow AIAA.

"physical" picture of the flowfield associated with spinning and nonspinning axisymmetric bodies so that improved flow models can be developed.

Description of Wind Tunnel and Associated Equipment

The experiments presented were conducted in one of the University of Notre Dame's low-turbulence subsonic smoke wind tunnels. The indraft wind tunnel used is shown in Fig. 1. The test section is equipped with a plate glass front, a black velvet-covered back, and interchangeable plate glass/solid wood parts along the top and bottom, allowing for a variety of lighting and measurement probe arrangements. The wind tunnel in this configuration can achieve velocities in the range of 5-27 m/s with a turbulence intensity of approximately 0.10% over this entire velocity range.

Smoke is generated by a device which allows deodorized kerosene to drop onto electrically heated plates. The smoke is forced out of the generator through a heat exchanger and a filter bag before it enters the wind tunnel from upstream of the first screen. A more detailed description of these facilities and their development may be found in Ref. 18.

Still photography of the smoke flow is accomplished using a Graphlex 101×127 mm (4×5 in.) camera, synchronized with four high-intensity General Radio Type 1532 strobolumes and Kodak Royal-X film. High-speed movies are obtained using a Wollensak WF-3 Fastax camera. The Fastax camera has a speed range of 1500-7000 frames/s. A Red Lake Laboratories timing light generator is used in conjunction with the Fastax camera to mark the film for accurate determination of the film speed.

Velocity profiles in the boundary layer were obtained using a DISA 55 M10 hot-wire anemometer and DISA Type 55 D10 linearization circuit. A DISA traversing mechanism allowed resolution of the position of the hot wire in the boundary layer to within ± 0.01 cm.

Description of Models

The baseline model for the flow visualization and pressure tests is an axisymmetric model consisting of a 3-caliber secant ogive nose, a 2-caliber cylindrical midsection, and a 1-caliber 7-deg conical boattail. Two baseline models were constructed; one to be used for the flow visualization and the other for measuring the pressure distribution of the body.

The flow visualization model was constructed of 6061T651 aluminum in three sections, as indicated in Fig. 2. This model was polished to a surface finish of 0.254 μm (10 μin.) and anodized black. The cylindrical midsection contains the bearings, mounting supports, and air turbine for the spin experiments. The midsection is internally threaded on both ends to allow easy interchange of the nose and boattail configurations.

The pressure model was identical to the flow visualization model, except that it was not anodized. This model was designed to have 48 pressure taps located axially along the surface, including a single base pressure tap. The pressures are measured using a Model 48J-9 Scanivalve and Setra Systems, Inc. Model 237 pressure transducer located inside the midsection of the model, as illustrated in Fig. 3. The pressure transducer was calibrated in the range $\pm 1.72 \times 10^3$ N/m^2 (± 0.25 psid) by the manufacturer.

The major difficulty in obtaining quality flow visualization still photographs and motion pictures is getting sufficient light on the subject of interest. This is particularly critical for the high-speed motion pictures. This difficulty was partially overcome through the use of four 2000 W high-intensity General Electric spotlights. Because of the short exposure time and lighting difficulties, the still and motion picture negatives were underexposed. To have sufficient contrast in the negatives the film must be overdeveloped.

Another problem encountered in high-speed smoke photography is the nonuniformity of the smoke density within the various stages of the boundary layer. The smoke patterns

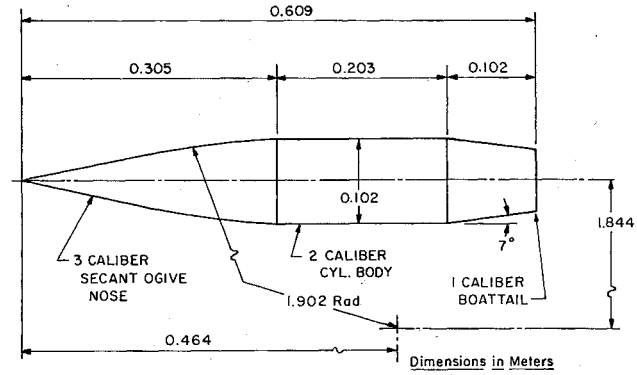

Fig. 2 Baseline secant-ogive nose flow visualization model. (All dimensions in meters.)

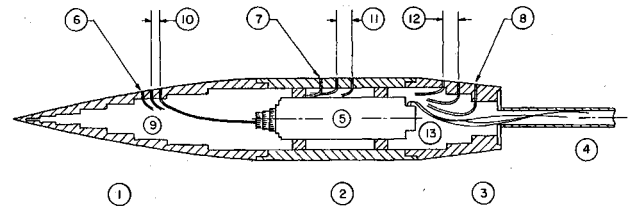

1. SECANT OGIVE NOSE
2. CYLINDRICAL BODY
3. BOATTAIL
4. STING
5. SCANIVALVE
6. 30 PRESSURE TAPS 1.27 m.m. I.D.
7. 12 PRESSURE TAPS
8. 6 PRESSURE TAPS
9. 1.27 m.m. I.D. TYGON TUBING
10. 10.16 m.m.
11. 20.32 m.m.
12. 20.32 m.m.
13. SCANIVALVE WIRES

Fig. 3 Baseline secant-ogive pressure model.

produce negatives with strong and faint images. If such negatives were printed in a conventional manner, the faint images (photographic data) would be lost. To avoid this problem, the positive prints require photographic dodging. This is a technique in which the print is unevenly exposed so that all the details in the negative are captured on the positive prints. To enhance the three-dimensional appearance as well as eliminate reflective glare from the high-intensity lighting, the camera was placed 30 deg from the perpendicular to the model. The high-intensity lights were placed on both sides of the camera.

Results

The ultimate objective of this boundary-layer study is to develop a physical picture of the flowfield associated with spinning and nonspinning axisymmetric bodies. It is hoped that this physical picture of the boundary-layer flow will lead to improved flowfield models.

The research was conducted in two phases. The first phase was the investigation of the boundary-layer development on the nonspinning body at zero angle at attack. During the second phase, the effect of spin on the boundary layer was documented.

Phase I. Nonspinning Model at Zero Angle of Attack

Flow visualization and pressure data were obtained on the baseline model for Reynolds numbers (based upon model length) from 0.315 to 1.03×10^6. Although this was a rather narrow range of Reynolds numbers, the phenomena occurring on the model varied dramatically.[19] At the lowest Reynolds number, 0.315×10^6, the flow remained laminar over the entire body. At about 0.75 caliber down the boattail, as shown in Fig. 4a, axisymmetric vortex rings were formed periodically and moved downstream into the wake. The rings were formed at a frequency of approximately 120 rings/s. A very slow recirculation region was visible near the surface of the boattail indicating that separation apparently took place shortly downstream of the boattail junction with the midsection.

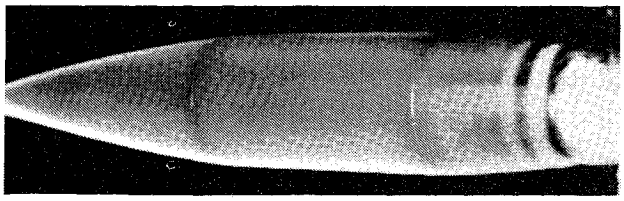

a) $Re_L = 0.315 \times 10^6$.

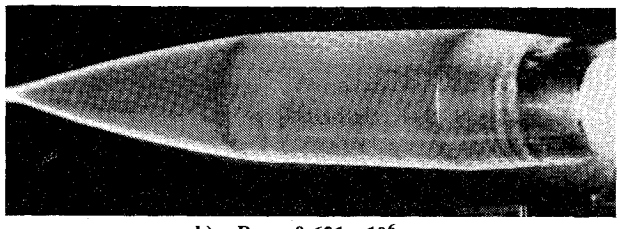

b) $Re_L = 0.631 \times 10^6$.

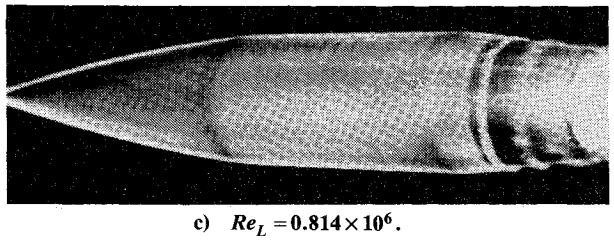

c) $Re_L = 0.814 \times 10^6$.

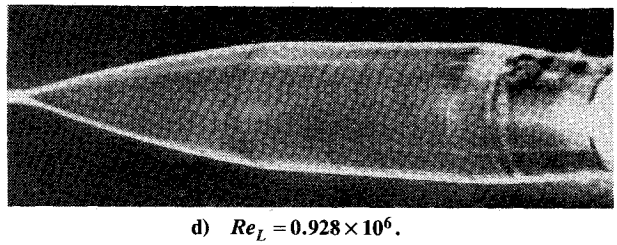

d) $Re_L = 0.928 \times 10^6$.

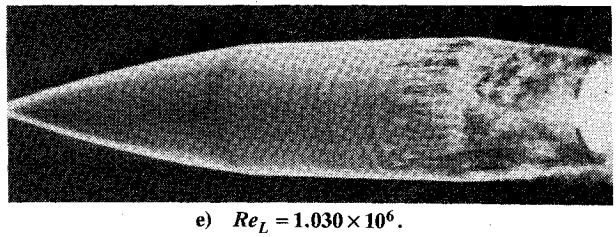

e) $Re_L = 1.030 \times 10^6$.

Fig. 4 Smoke photographs for various Reynolds numbers.

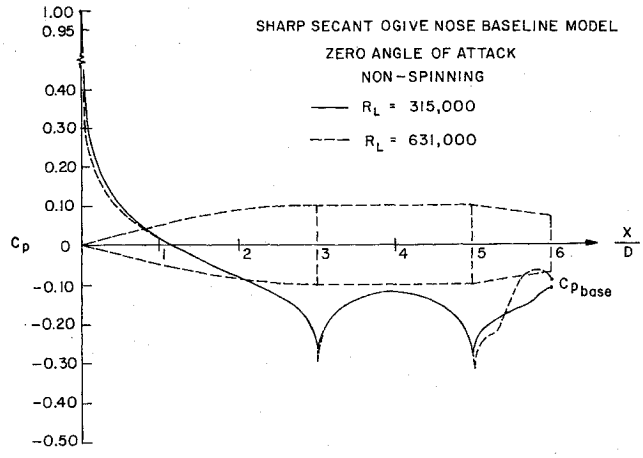

Fig. 5a Pressure distribution along the baseline model at zero angle of attack ($Re_L = 0.315$ and 0.631×10^6).

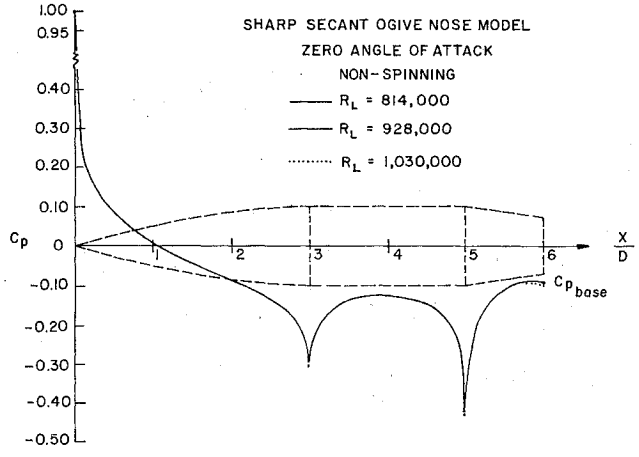

Fig. 5b Pressure distribution along the baseline model at zero angle of attack ($Re_L = 0.814$, 0.928, and 1.030×10^6).

For the Reynolds number 0.631×10^6 flow, two-dimensional Tollmien-Schlichting waves were observed intermittently along the cylindrical body. These waves disappeared as they approached the body-boattail intersection. It was observed that the point at which the axisymmetric vortex rings became visible had moved up the boattail to about 0.5 caliber, as shown in Fig. 4b. The axisymmetric vortex rings were formed as before; however, they accelerated more rapidly into the freestream just after separation. As shown in Fig. 5a, there is a marked difference in the pressure profiles along the boattail for the two lower Reynolds number flows.

At a Reynolds number of 0.814×10^6, two-dimensional Tollmien-Schlichting waves were observed continuously at the midpoint along the body and disappeared continuously just before the boattail. The appearance of vortex rings occurred at a position about 0.3 caliber along the boattail as illustrated in Fig. 4c. The vortex pattern was quite similar to that for the Reynolds number 0.631×10^6 flow; however, the rings broke down earlier into a turbulent wake. At a Reynolds number of 0.928×10^6, two-dimensional Tollmien-Schlichting waves formed continuously. Approximately 50% of these waves broke down to form vortex truss patterns. Vortex trusses are a result of a nonlinear three-dimensional deformation of the somewhat larger amplitude Tollmien-Schlichting waves. The highest points of the deformations are carried downstream faster than the portions of the waves that remain lower in the boundary layer, yielding a triangular or trussed appearance. The flow along the boattail became turbulent following the intermittent formation of the trusses. When trusses did not appear, axisymmetric vortex rings moved downstream and broke down rapidly, as shown in Fig. 4d.

At the highest Reynolds number studied, $Re_L = 1.03 \times 10^6$, the transition process was found to be similar to the results obtained by Brown[14] and Knapp and Roach[17] on a *tangent-ogive* nose body. The development of the transition process on a tangent-ogive nose axisymmetric body is illustrated in Fig. 6. For the highest Reynolds number all phases of the transition process were present. Figure 4e is a photograph of the boundary layer at the highest Reynolds number.

The transition phenomenon was observed and recorded through high-speed smoke photography. Hot-wire surveys of the boundary layer were taken at 0.5-caliber intervals along the body for $Re_L = 1.03 \times 10^6$. The boundary-layer thickness δ, where the Tollmien-Schlichting waves first become visible, was found to be 1.35 mm. The two-dimensional waves, region R_1 of Brown, were first observed at the midsection of the cylindrical portion of the model. It usually appeared that

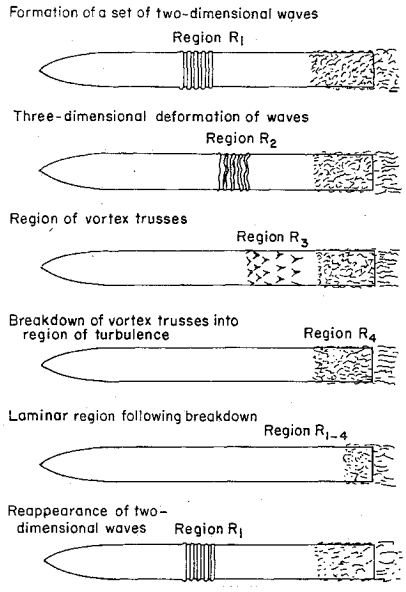

Fig. 6 Time development of boundary-layer transition (one cycle).[14]

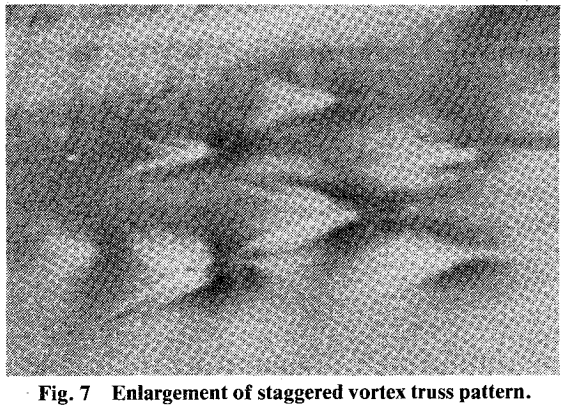

Fig. 7 Enlargement of staggered vortex truss pattern.

three to five strong (i.e., larger amplitude) waves were formed, followed by two to three weaker ones. Depending on the amplitude of the two-dimensional waves, trusses (region R_3 of Brown) were formed where $3.9 < Z/D < 4.75$, along the midsection of the body. Region R_2 of Brown, the three-dimensional deformation of the waves, was not always visible since the flow passes through this region to the truss formation stage quite rapidly. The average wave spacing was found to be approximately 9.9δ/wave. However, this wavelength was found to range from 8.4δ to 11.3δ. The wave speed was estimated to be about 10 m/s for the freestream velocity of 25.5 m/s or $0.39U_\infty$, in agreement with Ref. 20. It was observed that almost all the two-dimensional waves became three-dimensionally unstable and formed truss patterns before leaving the cylindrical portion of the model. However, approximately one in twenty did not form trusses and was simply washed downstream.

Groups of two to five two-dimensional waves, almost simultaneously, became unstable and formed trusses. Because the breakdown of the two-dimensional waves occurred so rapidly, the three-dimensional wave pattern observed by Brown was only apparent in some of the photographs. Approximately 90% of the trusses which were formed were arranged in a staggered formation, as shown in Fig. 7. The truss formation was immediately followed by a breakdown in the truss structure and the diffusion of the smoke into the developing turbulent boundary layer. This is illustrated in Fig. 8. It is well known that sound can influence Tollmien-Schlichting wave formation.[20,21] It was observed during preliminary testing of the influence of acoustic enhancement

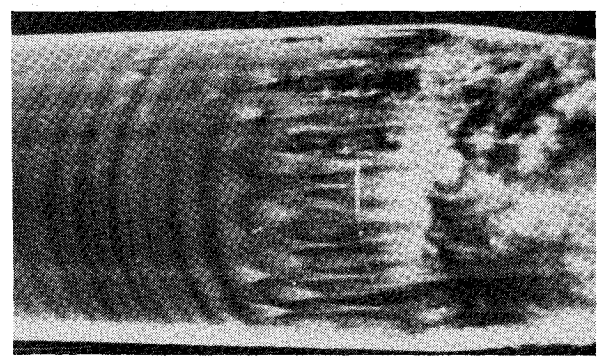

Fig. 8 Enlargement of transition region.

of amplitude of the Tollmien-Schlichting waves at $Re_L = 1.03 \times 10^6$ that the wavelength, λ_{TS}, could be varied from approximately 8.3 mm at 1200 Hz to approximately 21 mm at 460 Hz. In all cases the truss wavelength was approximately equal to the Tollmien-Schlichting wavelength. As the Tollmien-Schlichting wavelength decreased, the spacing between trusses also decreased and the truss pattern changed dramatically from a staggered to an in-line formation.

The pressure distributions for all five Reynolds numbers are very similar, with the only significant difference occurring along the boattail. The pressure distributions shown in Fig. 5b are typical for this model configuration. The C_p is equal to 1 at the tip of the nose and decreases continuously along the nose. A sharp spike in the pressure distribution occurs at the nose-body intersection. The pressure then increases along the center body, reaching a maximum at the midpoint. This adverse pressure gradient is favorable to the amplification of disturbances in the boundary layer. This is the region where the two-dimensional waves were observed in the smoke pictures for all but the lowest Reynolds number flow. The pressure distribution has a second and larger spike at the juncture between the body and the boattail. This spike indicates that the flow is accelerating in the locally favorable pressure gradient upstream of the boattail shoulder. This is demonstrated in the smoke pictures by the stretching of the vortex truss patterns at higher Reynolds numbers. As mentioned, there are significant differences in both the pressure data and the observed phenomena along the boattail at the Reynolds numbers 0.315×10^6 and 0.631×10^6. The higher Reynolds numbers produce approximately the same pressure profiles, except along the boattail as shown in Fig. 5.

Phase II. Spinning Model at Zero Angle of Attack

Still photographs were taken of the baseline model at zero angle of attack over a Reynolds number range from 0.315-1.030×10^6, and spin rates from 0-4500 rpm.[22] The transition process over the spinning model took a vastly different form than that of the nonspinning case. On the nonspinning model a viscosity conditioned instability leads to the development of two-dimensional Tollmien-Schlichting waves and their breakdown. The transition process on the spinning model bears resemblance to instabilities which occur on both the rotating disk[23] and the swept wing.[24] A typical example of this spin-induced transition process is shown in Fig. 9. The phenomenon was primarily related to the ratio of the peripheral velocity to the freestream velocity, V/U_∞, and relatively independent of Reynolds numbers (i.e., it was not significantly affected by changes in Reynolds number for a given V/U_∞). Experiments were conducted for a range of V/U_∞ between 0 and 1.67. There were no visible changes in the boundary-layer characteristics for V/U_∞ less than 0.4, with the exception of a slight skewness in the tips of the vortex trusses. When vortex trusses were present, this skewness could be seen for V/U_∞ values as low as 0.1, as shown in Fig. 10. As V/U_∞ increased striations in the smoke appeared at an angle approximately equal to $\tan^{-1}$ of $(-V/U_\infty)$, as shown in Fig.

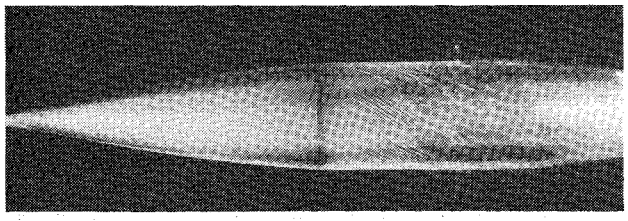

Fig. 9 Spin induced transition at zero angle of attack ($V/U_\infty = 0.658, Re_L = 0.928 \times 10^6$).

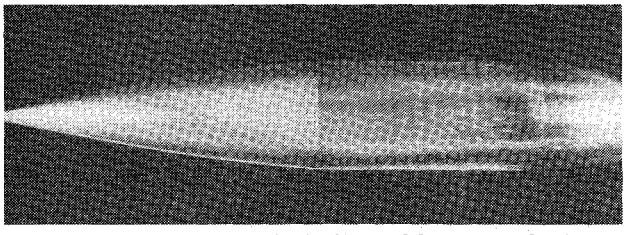

Fig. 10 Smoke photograph of spinning model at zero angle of attack ($V/U_\infty = 0.119, Re_L = 1.030 \times 10^6$).

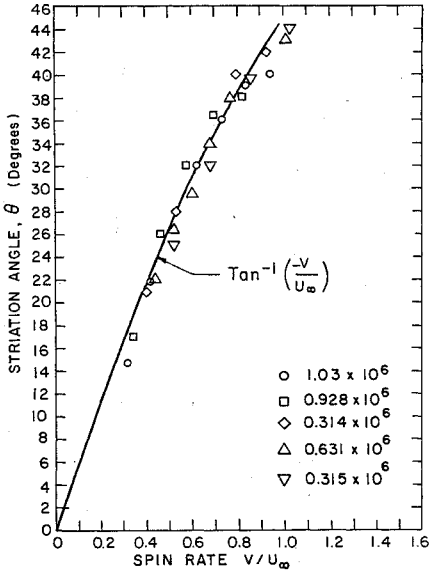

Fig. 11 Plot of measured striation angle vs spin rate.

11. As on swept wings, the striations are a manifestation of the inflectional or cross-flow instability; high-speed movies show vortices that appear to rotate in the same direction. Although a centrifugal instability probably contributes to the effect,§ evidently the cross-flow instability dominates in this case. The wavelength of these striations was on the order of the boundary-layer thickness and remained constant regardless of spin ratio V/U_∞. As the Reynolds number was increased, the transition process took place over a shorter distance. High-speed motion pictures suggest the presence of helicoidal disturbances along the vortex lines just prior to the onset of turbulence. Helicoidal disturbances can be discerned as corkscrew deformations of the striations in Fig. 12. High-speed smoke-flow movies showed that these disturbances, which traveled along the vortices, deformed with the same sense of rotation.

The direction of rotation of the model is not obvious from the appearance of the striations. If one were to leave a trail on the model with a paint brush, moving the brush only in the

§This possibility was suggested by Dr. W. Pfenninger, NASA Langley, Hampton, Virginia.

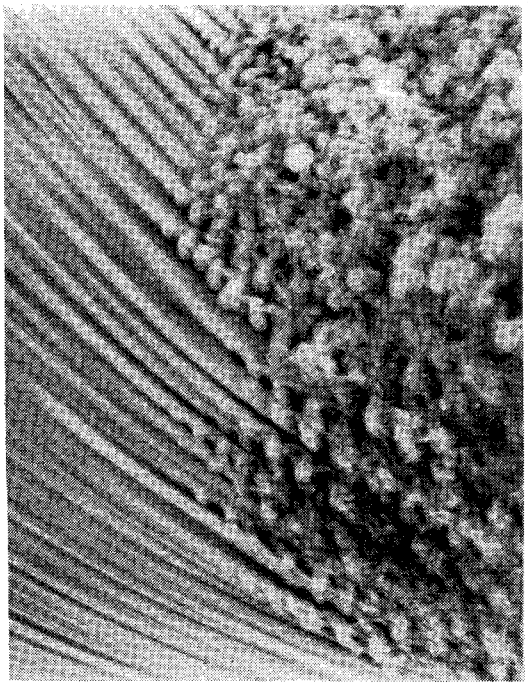

Fig. 12 Enlargement of striations illustrating striation breakdown ($V/U_\infty = 0.825, Re_L = 0.814 \times 10^6$).

direction of the freestream (from nose to tail) while the model was spinning clockwise (viewed from the rear), one would leave a trail along the model at the striation angle, approximately $\tan^{-1}(-V/U_\infty)$. However, the striations are not on the surface of the model. These striations are vortex lines with a sense of rotation opposite from that of the model. They are expected to form at a distance from the model near where the cross-flow velocity profile has an inflection point and becomes unstable. Figure 12 suggests that this locus, which approximately defines the origin of the spiral vortices, rotates with the body.

The location of the transition zone is largely a function of V/U_∞. For a constant rpm the transition zone moved forward with decreasing Reynolds number, just the opposite from what occurred on the nonspinning model. The transition zone moved forward with increasing spin rate as anticipated at a constant Reynolds number. Furthermore, when the striations appeared toward the end of the midsection, they were superimposed on the two-dimensional axisymmetric Tollmien-Schlichting waves. The simultaneous occurrence of the Tollmien-Schlichting waves and the vortices spiraling around the body, to the authors' knowledge, were first observed in the Notre Dame smoke tunnel.[25] These phenomena are the subject of further study. At high values of V/U_∞ (V/U_∞ greater than 1.0) the boundary layer was fully turbulent along the entire midsection over the range of Reynolds numbers studied.

Discussion of Results

Phase I. Nonspinning Model at Zero Angle of Attack

At least three different modes of transition to turbulence are observed over the range of conditions portrayed in Fig. 4. The three types which occur over the cylindrical part of the body start with two-dimensional Tollmien-Schlichting waves. Depending upon the Tollmien-Schlichting amplitudes reached for $4 < Z/D < 5$, the waves may:

1) Stop growing in the locally favorable pressure gradient and thus constitute initial disturbances for the locally or fully separated boundary layers over the boattail.

2) For somewhat larger amplitudes a secondary instability takes place, leading to *staggered* truss formations seen in Figs. 7 and 8.

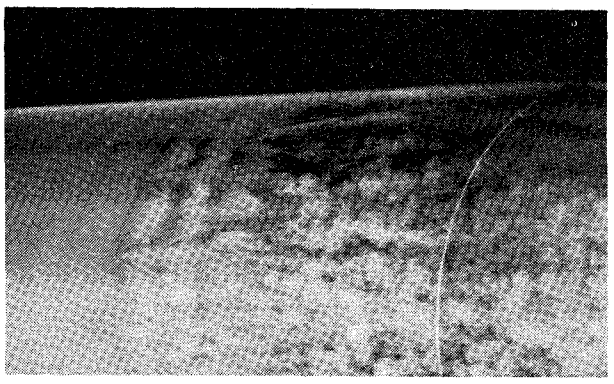

Fig. 13 Smoke photograph of nonspinning model at zero angle of attack showing aligned vortex trusses ($Re_L = 1.030 \times 10^6$), no acoustic enhancement.

3) When still larger amplitudes are reached in-line trusses are formed, as in Fig. 13.

Recently Kegelman[26] was able to change the staggered patterns to in-line patterns by acoustic enhancement of amplitude, all other conditions remaining unchanged. The staggered formations have presented a puzzle ever since they were observed by Brown[14] and Knapp and Roach.[17] The key to the identification is the recognition that along a streamline through the apices the visible wavelength suddenly doubles from the upstream λ_{TS} of the growing Tollmien-Schlichting waves. Hot-wire anemometry confirms that a sudden spectral growth near half of the Tollmien-Schlichting frequency accompanies the λ doubling. Recent combined hot-wire smoke-wire studies by Thomas and Saric,[27] Saric et al.,[28] and Kachanov and Levchenko[29] showed the staggered wave formation to be consistent with the mechanism of nonlinear triad resonance described by Craik[30] in 1971. Recently Herbert[31] described another subharmonic mechanism, also consistent with the present visual and hot-wire information. Detailed profile measurements of spanwise or normal fluctuations will be needed to distinguish unequivocally between the two theories.

When the initial two-dimensional Tollmien-Schlichting wave of frequency f grows to a threshold magnitude, towards the end of its passage through the region of amplification of linear stability theory, it may pass energy, nonlinearly and rather rapidly, to skew vorticity waves of frequency $f/2$. Such skew waves are visible in the nonlinear region as the legs of the staggered trusses in Figs. 7 and 8. According to Saric,[32] the threshold value may be as low as $0.003U_\infty$. The waves in Figs. 4b and 4c are below this threshold value for $Z/D<5.0$. The significance of the present results is that the Craik or Herbert resonance, case 2, occurs *without* artificial stimulation of the initial Tollmien-Schlichting wave by a vibrating ribbon (which was used in the Thomas-Saric-Kachanov experiments).

When in-line trusses are observed, case 3, as in Fig. 13, the nonlinear breakdown apparently also involves skew waves, but of the frequency f rather than $f/2$. Although hairpin eddies are seldom detectable, there is little doubt that this breakdown is topologically the same as that described by Klebanoff et al.[33] and visualized by Hama and Nutant.[34] In our experiments the Klebanoff breakdown is observed at higher Reynolds numbers without artificial excitation, as in Fig. 13.

At intermediate Reynolds numbers the Craik or Herbert $f/2$ subharmonic resonance can be pre-empted by exciting the amplitude acoustically past another threshold value on the order of $0.01U_\infty$. Evidently the damping past the upper neutral curve of the linear stability theory is no longer operative at such amplitudes and is replaced by a secondary instability different from Craik or Herbert.

In case 1, Figs. 4b and 4c, the small Tollmien-Schlichting vorticity distributions arriving at $Z/D=5$, do not correspond to the modes of instability over the boattail. The laminar boundary layer separates at the shoulder, creating a highly inflectional profile which is very unstable. The distributed vorticity rolls up into clearly identifiable rather axisymmetric vortex rings, somewhat hampered by the proximity of the wall. The associated entrainment usually causes a reattachment of the flow, laminar or turbulent, forming a so-called laminar bubble. The onset of turbulence for such geometries is apparently closer to that in free-mixing layers (such as described by Miksad[35] and Freymuth[36]) than to the sudden local turbulent three-dimensional spot formations as expected for case 3 in later stages of the Klebanoff in-line breakdown. Our present observations are consistent with the more gradual development of randomness described by Arnal and Juillen[37] and Gleyzes et al.[38] for various geometries of laminar bubbles. The latter reference suggests that the rolled up vortices may pair even though the flow is reattaching. Thus our geometry exhibits at least three different types of breakdown modes leading to wall turbulence for the nonspinning case over the range of Reynolds numbers studied.

Phase II. Spinning Model at Zero Angle of Attack

The smoke visualization of the spinning model at zero angle of attack shows the following effects as spin rate is increased. An inflectional cross-flow instability generates vortices that spiral around the body, yielding a striated appearance to the smoke in the boundary layer, when the spin rate is greater than $V/U_\infty = 0.4$. When the spin rate is less than 0.4, only a skewness in the tips of the trusses can be observed when trusses are present. The formation of cross-flow vortices is primarily dependent upon the nondimensional spin rate, V/U_∞, and relatively independent of Reynolds number over the range used. The entire transition process does take place over a slightly shorter region when the Reynolds number is increased. The striations break down possibly after a helical instability. The boundary layer along the midsection of the model is entirely turbulent for values of V/U_∞ greater than 1.0.

The results presented are part of a continuing research program to develop a better understanding of the complicated boundary-layer development on a spinning axisymmetric body. Present and future studies will investigate the boundary layer and Magnus force on the body at angle of attack for various nose bluntness geometries. The influence of sound on the transition process also will be studied.

Acknowledgments

This research effort was supported by the United States Army Research Office under Grant DAAG-29-78-G-0102 and the Department of Aerospace and Mechanical Engineering. The authors would especially like to thank Prof. Mark V. Morkovin for his suggestions and encouragement throughout this project and for his help in relating this research to the results of other investigators. The authors would also like to thank Prof. Eli Reshotko for his helpful comments on this manuscript.

References

[1] Martin, J. C., "On the Magnus Effects Caused by the Boundary Layer Displacement Thickness on Bodies of Revolution at Small Angles of Attack," Ballistics Research Laboratories, Rept. 870, June 1955.

[2] Vaughn, H. R. and Reis, G. E., "A Magnus Theory for Bodies of Revolution," Sandia Laboratories, SC-RR-720537, Jan. 1973.

[3] Lin, T. C. and Rubin, S. G., "Viscous Flow Over Spinning Cones at Angle of Attack," *AIAA Journal*, Vol. 12, July 1977, pp. 965-974.

[4] Dwyer, H. A. and Sanders, B. R., "Magnus Forces on Spinning Supersonic Cones—Part I: The Boundary Layer," *AIAA Journal*, Vol. 14, May 1976, pp. 576-582.

[5] Sanders, B. R. and Dwyer, H. A., "Magnus Forces on Spinning Supersonic Cones—Part II: Inviscid Flow," *AIAA Journal*, Vol. 14, May 1976, pp. 576-582.

[6]Graff, G. Y. and Moore, F. G., "The Effect of Boattail Shape on Magnus," NSWC/DL TR-3581, Dec. 1976.

[7]Morton, J. B., Jacobson, I. D., and Sanders, S., "Experimental Investigation of the Boundary Layer on a Rotating Cylinder," University of Virginia, SS-3318-112-74, May 1974.

[8]Sturek, W. B., "Boundary Layer Studies on a Spinning Tangent-Ogive Cylinder Model," Ballistics Research Laboratories, Rept. 1801, July 1975.

[9]Sturek, W. B., Dwyer, H. A., Kayser, L. D., Nietubicz, C. J., and Reklis, R. P., "Computations of Turbulent Boundary Layer Development Over a Yawed, Spinning Body of Revolution with Application to Magnus Effect," Ballistics Research Laboratories, Rept. 1985, May 1977; also, *Proceedings of Symposium on Turbulent Shear Flows,* Pennsylvania State University, April 1977, pp. 9.37-9.45.

[10]Archarya, M., "Effect of Compressibility on Boundary Layer Turbulence," *AIAA Journal*, Vol. 15, March 1977, pp. 303-304.

[11]Reshotko, E., "A Program for Transition Research," *AIAA Journal*, Vol. 13, March 1975, pp. 261-265.

[12]Morkovin, M. W., "Technical Evaluation Report of the Fluid Dynamic Panel Symposium on Laminar-Turbulent Transition," AGARD, AR-122, June 1978.

[13]Nagamatsu, H. T., Wisler, D. C., and Shear, R. E. Jr., "Circumferential Nonuniform Heating during Transition on a Slender Cone at Hypersonic Mach Numbers," General Electric Co., Rept. 67-C-272, July 1967.

[14]Brown, F. N. M., "The Physical Model of Boundary Layer Transition," *Proceedings of Ninth Midwestern Mechanics Conference,* University of Wisconsin, Aug. 1965, pp. 421-429.

[15]Knapp, C. F., "Analysis of Natural Boundary Layer Transition," *AIAA Student Journal*, Vol. 4, Dec. 1966, pp. 147-152.

[16]Knapp, C. F., Roache, P. J., and Mueller, T. J., "A Combined Visual and Hot-Wire Anemometer Investigation of Boundary Layer Transition," University of Notre Dame, UNDAS-TR-866CK, Aug. 1966.

[17]Knapp, C. F. and Roache, P. J., "A Combined Visual and Hot-Wire Anemometer Investigation of Boundary Layer Transition," *AIAA Journal*, Vol. 6, Jan. 1968, pp. 29-36.

[18]Mueller, T. J., "Smoke Visualization of Subsonic and Supersonic Flows (The Legacy of F. N. M. Brown)," University of Notre Dame, UNDAS-TN-3412-1, Aug. 1979.

[19]Kegelman, J. T., Nelson, R. C., and Mueller, T. J., "Smoke Visualization of the Boundary Layer on an Axisymmetric Body," AIAA Paper 79-1635, Aug. 1979.

[20]Schlichting, H., *Boundary Layer Theory*, 7th ed., McGraw Hill Book Co., New York, p. 476.

[21]Brown, F. N. M. and Goddard, V. P., "The Effect of Sound on the Separated Laminar Boundary Layer," National Science Foundation, Contract NSF-G-11712, 1963.

[22]Kegelman, J. T., Nelson, R. C., and Mueller, T. J., "Boundary Layer and Side Force Characteristics of a Spinning Axisymmetric Body," AIAA Paper 80-1584-CP, Aug. 1980, pp. 236-250.

[23]Gregory, N., Stuart, J. T., and Walker, W. S., "On the Stability of Three-Dimensional Boundary Layers with Application to the Flow Due to a Rotating Disk," *Transactions of the Royal Society of London*, Series A, Vol. 248, 1955, pp. 155-199.

[24]Poll, D. I. A., "Three-Dimensional Boundary Layer Transition via the Mechanisms of Attachment Line Contamination and Cross-Flow Instability," Cranfield College of Aeronautics, England, Rept. 7904, Sept. 1979.

[25]Mueller, T. J., Nelson, R. C., Kegelman, J. T., and Morkovin, M. V., "Smoke Visualization of the Boundary Layer on a Spinning Axisymmetric Body," *AIAA Journal*, Vol. 19, Dec. 1981, pp. 1607-1608.

[26]Kegelman, T., "Experimental Studies of Boundary Layer Transition on a Spinning and Non-Spinning Axisymmetric Body," Ph.D. Dissertation, Department of Aerospace and Mechanical Engineering, University of Notre Dame, Notre Dame, Ind., Sept. 1982.

[27]Thomas, A. S. W. and Saric, W. S., "Harmonic and Subharmonic Waves During Boundary-Layer Transition," *Bulletin of the American Physical Society*, Vol. 26, No. 9, 1981, p. 1252.

[28]Saric, W. S., Carter, J. D., and Reynolds, G. A., "Computation and Visualization of Unstable-Wave Streaklines in a Boundary Layer," *Bulletin of the American Physical Society*, Vol. 26, No. 9, 1981, p. 1252.

[29]Kachanov, Yu S. and Levchenko, V., " Resonant Interaction of Disturbances in Boundary Layers during Transition to Turbulence," Preprint 10-82, Institute of Theoretical and Applied Mechanics, Soviet AC.Su., Novosibirsk, U.S.S.R., 1982.

[30]Craik, A. D., "Nonlinear Resonant Instability in Boundary Layers," *Journal of Fluid Mechanics*, Vol. 50, Pt. 2, 1971, pp. 393-413.

[31]Herbert, T., "Secondary Instability of Plane Channel Flow to Subharmonic Three-Dimensional Disturbances." *Physics of Fluids*, Vol. 26, No. 4, April 1983, pp. 871-874.

[32]Saric, W. S., Private communication, Virginia Polytechnic Institue and State University, Blacksburg, Va., 1982.

[33]Klebanoff, P. S., Tidstrom, K. D., and Sargent, L. M., "The Three-Dimensional Nature of Boundary-Layer Instability," *Journal of Fluid Mechanics*, Vol. 12, Pt. 1, 1962, pp. 1-34.

[34]Hama, F. R. and Nutant, J., "Detailed Flow Field Observations of the Transition Process in a Thick Boundary Layer," *Proceedings of the Heat Transfer and Fluid Mechanics Institute*, Stanford University Press, Stanford, Calif., 1963, pp. 77-93.

[35]Miksad, R. W., "Experiments on the Nonlinear Stages of Free-Shear-Layer Transition," *Journal of Fluid Mechanics*, Vol. 56, Pt. 4, 1972, pp. 695-719.

[36]Freymuth, P., "On Transition in Separated Boundary Layers," *Journal of Fluid Mechanics*, Vol. 25, Pt. 4, 1966, p. 683.

[37]Arnal, D. and Juillen, J. C., "Results of Experiments Concerning the Influence of Transition on the Initial Structure of Turbulent Boundary Layers," ONERA TP 1979-128 (in French).

[38]Gleyzes, Ch., Coustein, J., and Bonnet, J.-L., "Laminar Bubbles with Transition to Turbulence—Theory and Experiment," *L'Aeronautique et l'Astronautique*, No. 80, 1980-1, pp. 41-57 (in French).